

Variational Spin-Squeezing Algorithms on Programmable Quantum Sensors

Raphael Kaubruegger^{1,2}, Pietro Silvi^{1,2}, Christian Kokail^{1,2}, Rick van Bijnen^{1,2}, Ana Maria Rey^{3,4}, Jun Ye³,
Adam M. Kaufman³ and Peter Zoller^{1,2}

¹Center for Quantum Physics, University of Innsbruck, Innsbruck A-6020, Austria

²Institute for Quantum Optics and Quantum Information of the Austrian Academy of Sciences, Innsbruck A-6020, Austria

³JILA, National Institute of Standards and Technology and University of Colorado and Department of Physics, University of Colorado, Boulder, Colorado 80309, USA

⁴Center for Theory of Quantum Matter, University of Colorado, Boulder, Colorado 80309, USA



(Received 2 September 2019; published 30 December 2019)

Arrays of atoms trapped in optical tweezers combine features of programmable analog quantum simulators with atomic quantum sensors. Here we propose variational quantum algorithms, tailored for tweezer arrays as programmable quantum sensors, capable of generating entangled states on demand for precision metrology. The scheme is designed to generate metrological enhancement by optimizing it in a feedback loop on the quantum device itself, thus preparing the best entangled states given the available quantum resources. We apply our ideas to the generation of spin-squeezed states on Sr atom tweezer arrays, where finite-range interactions are generated through Rydberg dressing. The complexity of experimental variational optimization of our quantum circuits is expected to scale favorably with system size. We numerically show our approach to be robust to noise, and surpassing known protocols.

DOI: [10.1103/PhysRevLett.123.260505](https://doi.org/10.1103/PhysRevLett.123.260505)

Optical tweezer arrays of neutral atoms provide a bottom-up approach to assemble and design quantum many-body systems “atom by atom.” The flexibility and universality of tweezers, as a novel tool to engineer atomic and molecular quantum devices, is demonstrated by recent experiments, which range from realization of “programmable” analog quantum simulators for spin-models in tweezer arrays [1–3], to first demonstrations of potential tweezer-based clocks [4–9]. Atomic many-body systems designed around tweezer platforms thus offer the unique possibility of combining, on the same physical device, programmability to generate many-particle entangled states, and adopting these states as a quantum resource in precision measurement, exhibiting quantum advantage provided by entanglement. With near future experiments promising a scaling to hundreds of atoms, the challenge is to design and run quantum algorithms that efficiently generate entangled states of interest for precision measurements, given the—in general nonuniversal—entangling resources available on “programmable” quantum sensors, and Rydberg tweezer arrays in particular.

Here we propose hybrid classical-quantum algorithms [10–22] to be run as a quantum feedback loop to generate the *best* entangled states for the given platform, yielding precision enhancement beyond the standard quantum limit (SQL) [23,24]. The variational many-body wave function is iteratively optimized on the quantum device itself, in terms of a relevant cost function quantifying the metrological enhancement. After optimization, the resulting optimal wave function can be reprepared on demand on the

quantum sensor [25], directly available for high precision measurement (see Fig. 1). Performing the optimization on the physical platform will yield the best entangled state achievable in the presence of the actual imperfections and noise, thus outperforming optimization loops purely based on numerical simulations [26]. Moreover, since near-term quantum devices are expected to soon operate in regimes beyond the reach of numerical simulations [27], the optimization loop can ultimately *only* be run directly on the programmable quantum sensor. In this work we specifically target the optimized preparation of spin-squeezed states (SSS) [24,28,29], a class of entangled states enhancing measurement precision of atomic Ramsey interferometers, as demonstrated in experiments [30–45], and in general phase estimation techniques required by atomic clocks.

Ramsey interferometry.—The Ramsey sequence, acting on a two-level atom, described by spin-1/2 states $\{|\downarrow_z\rangle, |\uparrow_z\rangle\}$, and corresponding spin operators $s \equiv \hbar(\sigma_x, \sigma_y, \sigma_z)/2$, starts with an initial $\pi/2$ pulse that creates a coherent superposition $(|\downarrow_z\rangle + |\uparrow_z\rangle)/\sqrt{2} = |\uparrow_x\rangle$. In the subsequent interrogation time, $|\downarrow_z\rangle$ and $|\uparrow_z\rangle$ acquire a relative phase φ , encoding the quantity to be measured. The final $\pi/2$ pulse transfers this phase difference into a measurable state population difference. In this context, SSS are a well-known family of entangled states enhancing the phase sensitivity over N uncorrelated atoms [28]. Here, we prepare SSS via an entangling squeezing operation $\mathcal{S}(\theta)$ realizable on the programmable quantum sensor [see Fig. 1(a)]. The variational quantum algorithm optimizes

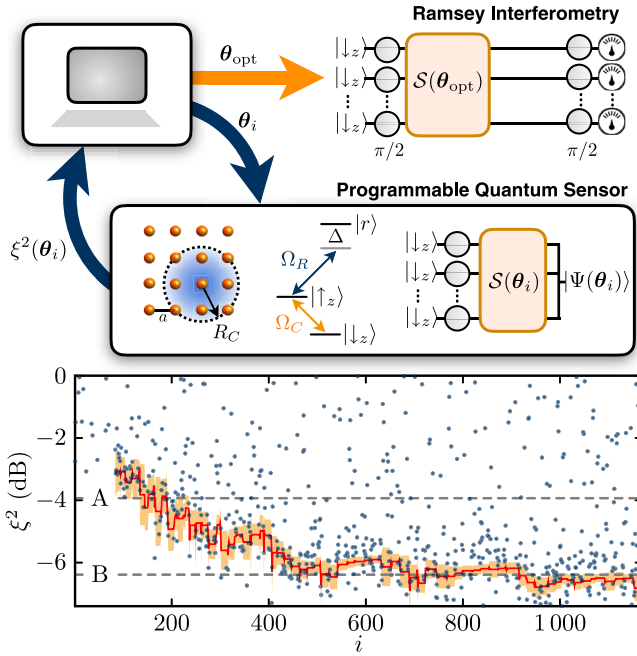


FIG. 1. Hybrid classical-quantum optimization on a programmable quantum sensor prepares spin-squeezed states for Ramsey interferometry. Variational control parameters θ generate trial states $|\Psi(\theta)\rangle = \mathcal{S}(\theta)R_y(\pi/2)|\downarrow_z\rangle^{\otimes N}$. The squeezing parameter $\xi(\theta)$ serves as cost function for classical optimization. Bottom: Optimization run on a 4×4 array with $R_C/a = 1.5$, using $\approx 10^5$ simulated experimental runs, showing measured spin-squeezing of the trial states (blue dots, one iteration = 100 measurements). A and B indicate theoretically obtainable squeezing with finite- and infinite-range one axis twisting [29,46], respectively. Red line and orange error band represent the predicted squeezing minima at iteration i of the search algorithm.

the classical control variables θ , parametrizing $\mathcal{S}(\theta)$, to achieve optimal spin squeezing.

Spin squeezing.—The achievable phase sensitivity $\Delta\varphi = \xi/\sqrt{N}$, is quantified by the spin squeezing parameter [28],

$$\xi^2(\theta) = N \frac{(\Delta J_{\perp, \min})_{\theta}^2}{|\langle \mathbf{J} \rangle_{\theta}|^2}, \quad (1)$$

to be minimized on the quantum sensor. Here $\mathbf{J} = \sum_{i=1}^N \mathbf{s}_i$ denotes the collective spin vector associated with an ensemble of N two-level atoms and $(\Delta J_{\perp, \min})_{\theta}^2 \equiv \langle J_{\perp, \min}^2 \rangle_{\theta} - \langle J_{\perp, \min} \rangle_{\theta}^2$ quantifies the minimal spin fluctuation orthogonal to the Bloch vector $\langle \mathbf{J} \rangle_{\theta}$. The expectation values in (1) are to be estimated, with respect to the variational wave function $|\Psi(\theta)\rangle = \mathcal{S}(\theta)|\uparrow_x\rangle^{\otimes N}$.

In atom-tweezer arrays, $\langle J_{\perp, \min}^2 \rangle_{\theta}$ is assembled from two-body correlation functions, directly measurable due to single site resolution.

Mechanisms known to generate spin squeezing are one-axis twisting $S_1(\tau) = \exp[-i\tau J_z^2]$ (OAT) and two-axis twisting (TAT) $S_2(\tau) = \exp[-i\tau(J_z^2 - J_y^2)]$ [29]. Various

theoretical studies [47–51] employ time-dependent dynamics to generate effective TAT, and more generally spin squeezing up to the Heisenberg limit $\xi^2 \simeq 1/N$. We note that these approaches rely on infinite-range interactions, conserving symmetries that constrain the dynamics to the particle permutation symmetric subspace, of linear dimension $(N+1)$, where the maximally SSS are known to be located [52–54]. In contrast, dynamics originating from *finite-range* interactions, such as Rydberg dressing, may explore an exponentially large Hilbert space.

Programmable quantum sensor.—The tweezer-based SR platform combines the advantages of a state of the art atomic clock [55,56], with the possibility of programming entangling operations [46]. Interactions among the atoms can be engineered via Rydberg dressing [57–65], where an off-resonant coupling $\Omega_R/\Delta \ll 1$ of the $|\uparrow_z\rangle$ clock level with a Rydberg state induces a distance-dependent pairwise energy shift. Here Ω_R denotes the Rabi frequency and Δ the detuning of the dressing laser. The resulting interaction Hamiltonian is of the form $H_D = \sum_{i,j < i} V_{ij} s_i^z s_j^z + \sum_i \delta_i s_i^z$, with effective site-dependent detunings $\delta_i = (-\Delta + \sum_{j \neq i} V_{i,j})/2$ and pairwise interaction potential

$$V_{ij} = V_0 \frac{R_C^6}{|r_i - r_j|^6 + R_C^6}, \quad (2)$$

between two particles at positions $\mathbf{r}_{i,j}$, where $V_0 = (\Omega_R/2\Delta)^3 \hbar \Omega_R$ and $R_C = |C_6/2\hbar\Delta|^{1/6}$ are related to the laser parameter and the C_6 van der Waals coefficient of the Rydberg state. The amount of spin squeezing generated from these *finite-range* interactions in a OAT protocol has been studied in Ref. [46], and we will refer to this as finite-range OAT (FOAT).

Below we design a variational circuit, $\mathcal{S}(\theta)$, to optimize spin squeezing from the physical resources described above. The circuit $\mathcal{S}(\theta) = \mathcal{U}_n, \dots, \mathcal{U}_1$ comprises a sequence of n unitary layers in which each \mathcal{U}_i is composed of quantum operations of the form

$$\mathcal{U}_i = D_x(\tau'_i) R_x(\vartheta_i) D_z(\tau_i), \quad (3)$$

with $\theta = \{\tau_1, \vartheta_1, \tau'_1, \dots, \tau_n, \vartheta_n, \tau'_n\}$. The fundamental building blocks of each layer are the interaction gates $D_{x,z}(\tau) = \exp[-i\tau \sum_{1 \leq i < j \leq N} V_{ij} s_i^{x,z} s_j^{x,z}]$, which can be obtained from the bare dressing in combination with global rotations $R_{x,y,z}(\vartheta_i) = \exp[-i\vartheta_i J_{x,y,z}]$ [54]. The design of this circuit and its building blocks is motivated by the following requirements. (i) The sequence is assembled from global gates only. Hence, the number of variational parameters ($3n$) does not increase with the system size N . (ii) The unitaries \mathcal{U}_i are designed to preserve the direction of the collective spin $\langle \mathbf{J} \rangle_{\theta} / |\langle \mathbf{J} \rangle_{\theta}|$ to be oriented along the x axis. This removes the overhead of determining the direction of the Bloch vectors via extra measurements after each variational step [54]. Equation (3) describes the most general gate sequence satisfying these requirements.

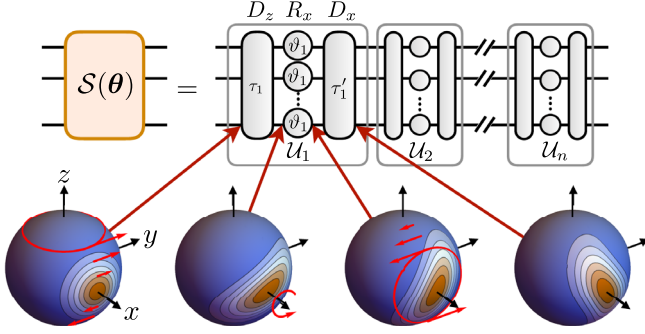


FIG. 2. Quantum circuit representing the variational squeezing operation. The squeezer $S(\theta)$ is a sequence of n unitary layers U_i ($i = 1, \dots, n$). Each U_i is further decomposed into two entangling interactions D_z and D_x and one global rotation R_x , as in Eq. (3), controlled by three variational parameters τ_i , θ_i , τ_i' . Typical Husimi distributions [54] of the quantum state before each gate, are displayed on a generalized Bloch sphere. The action of the gates onto the permutation invariant subspace is indicated by red arrows.

We visualize in Fig. 2 the action of the variational gate sequence, by means of the Husimi distribution plotted on a generalized Bloch sphere. The Husimi distribution displays the overlap of the time evolved state with coherent spin states with $|J| = N/2$ [54]. In this representation, a good SSS according to Eq. (1) forms a narrow vertical ellipse. The actions of the gates can now also be understood: D_z shears the Husimi distribution, the R_x gate performs rigid rotations, whereas D_x causes a winding around the x axis. Together, these transformations enable optimal spin squeezing while passing through transient nonelliptic states [66] (see fourth sphere in Fig. 2).

In the following, we quantify the spin squeezing, attainable by our variational ansatz on different tweezer array geometries. First, we numerically emulate the feedback loop optimization under realistic experimental conditions, imposing a finite number of experimental runs on the quantum device. Afterwards, we provide a more detailed analysis of the performance and robustness of the variational gate sequence.

2D arrays: single optimization run with shot noise.—We perform a numerical simulation of the feedback-loop optimization on a 4×4 square lattice with short-ranged interactions, where we chose a circuit depth of $n = 4$, corresponding to 12 variational parameters. During optimization, the cost function is estimated on the simulated experiment, as a statistical average over several runs. Each run consists of (i) preparation of the initial state $|\downarrow_z\rangle^{\otimes N}$, (ii) coherent quantum dynamics controlled by trial parameters θ_i of the current iteration i of the search algorithm, and (iii) quantum projective measurements, performed in parallel on every spin [all spins are measured in the same basis, either x or y , to estimate numerator and denominator of $\xi^2(\theta_i) = N \langle J_y^2 \rangle_{\theta_i} / \langle J_x \rangle_{\theta_i}^2$, respectively]. Figure 1 shows an optimization trajectory, employing 100 runs for a single

cost function evaluation, and restricting the total number of runs to $\sim 10^5$, compatible with current repetition rates of Sr tweezer platforms of ~ 1 Hz. The number of runs required for a single cost function evaluation at fixed precision does not increase with N [54]. Our analysis demonstrates that even in the presence of noisy cost function evaluations, we are able to obtain considerable spin squeezing, surpassing the squeezing attainable from infinite-range OAT, with short-ranged interactions. The optimization algorithm that we adopt is a modified version of the DIRECT algorithm [67–70], as has been implemented in experiments on hybrid quantum-classical simulation (see methods section in Ref. [20]).

2D arrays: exact results.—We now analyze the squeezing theoretically attainable with our variational circuit, at finite circuit depth n and interaction radius R_C . Figure 3 (top left panel) displays results from numerical optimization on a 4×4 square lattice, where we observe metrological enhancement over FOAT [46]. Our analysis reveals two distinct R_C regimes, roughly separated by the square array diagonal $R^* = \sqrt{18}a$, with $3a$ being the edge length. While for $R_C > R^*$ interactions are all to all and the particle

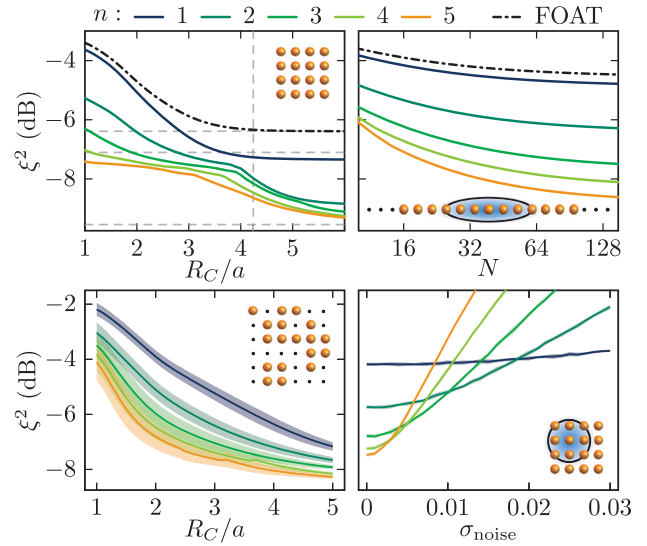


FIG. 3. Exact optimization results for circuit depths from $n = 1$ to 5 layers, compared with FOAT [46] (dot dashed line). Top left panel: optimized squeezing parameter ξ^2 in a 4×4 square array as a function of the interaction radius R_C/a . The vertical dashed line indicates the diagonal $R^* = \sqrt{18}a$, while the horizontal ones show, from top to bottom, the squeezing obtainable with OAT, TAT and the fundamental squeezing limit $\xi_{\text{lim}}^2(N) = [(2)/(N + 2)]$. Top right panel: optimized squeezing parameter in a 1D array, as a function of the particle number N , at fixed $R_C/a = 3$. Bottom left panel: optimization for a random realization, displayed in the inset, of a half-filled 6×6 square array. The data points display averages over various random half-filling realizations, at the optimal pulse sequence. Bottom right panel: impact of normally distributed control noise fluctuating with a relative standard deviation σ_{noise} around the optimal values.

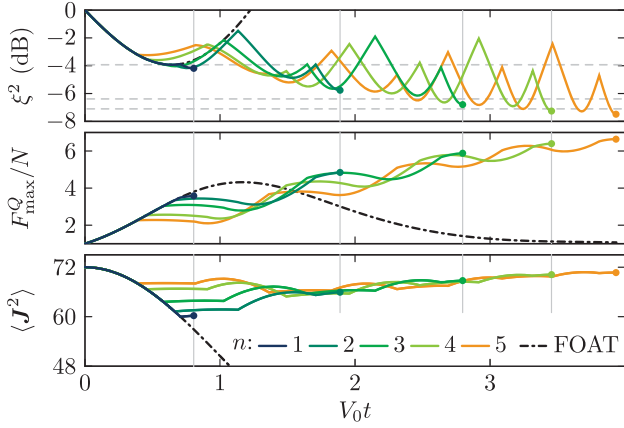


FIG. 4. Real-time dynamics of optimized pulse sequences, with different squeezer depths n on a 4×4 square array ($R_C/a = 1.5$). Rotation pulses are treated as instantaneous, so that $t \in [0, \sum_{i=1}^n (\tau_i + \tau'_i)]$ captures the cumulated interaction time. Dot-dashed lines show evolution under a single D_z interaction. The displayed quantities are the (rotationally invariant) spin squeezing ξ^2 (top panel), quantum Fisher information F_{\max}^Q/N (middle) and total angular momentum $\langle J^2 \rangle$ (bottom). The horizontal dashed lines in the top panel correspond to the spin squeezing obtainable with FOAT, infinite-range OAT and TAT, respectively, top to bottom. Vertical lines mark total interaction time for various circuit depths.

permutation symmetry is approximately protected, for $R_C < R^*$ the variational ansatz covers an exponentially large Hilbert space, and restoring the symmetry requires deeper circuits. This property is clearly visible in Fig. 4, where three quantities are plotted as a function of the effective interaction time during an optimized evolution, for $R_C/a = 1.5$. The bottom panel tracks the total angular momentum $\langle J^2 \rangle$, which stays large and recovers values close to its maximum $\max \langle J^2 \rangle = (N/2 + 1)N/2$, indicating a restoration of permutation symmetry. The top panel displays the spin squeezing parameter. We observe that the variational state passes through intermediate states with reduced squeezing, eventually surpassing the squeezing limits of FOAT, OAT, and TAT for sufficiently large depths n . In the middle panel we plot the quantum Fisher information (QFI) $F_{\max}^Q = \max_n [(4)/(|n|^2)] [\langle (\mathbf{n} \cdot \mathbf{J})^2 \rangle - \langle \mathbf{n} \cdot \mathbf{J} \rangle^2]$, a measure of metrological enhancement [71] and a witness for k -partite entanglement if $F_{\max}^Q/N > k$ [72,73]. We observe that, compared to ξ^2 , the QFI is a smoother function of time, a hint that the optimal evolution passes through transient non-Gaussian states [54].

1D arrays.—In order to investigate the performance of the protocol at large particle numbers, in Fig. 3 (top right panel) we show numerical simulations on 1D arrays up to 150 sites at fixed $R_C/a = 3$. Since the low connectivity of 1D systems yields slow entanglement generation, a power-law scaling of the squeezing parameter $\xi^2(N)$ with the system size at a finite R_C is not expected [46,74] and the squeezing will be below the one obtainable in either 2D or

3D arrays. However, the 1D geometry allows the simulation of large system sizes using matrix product states (MPS) [75]. The plot displays the optimized spin squeezing as a function of the particle number. We observe moderate improvement when more particles are added to the system. Instead, significantly more spin squeezing is generated if the circuit depth is increased. We expect this to hold also for higher dimensional systems. Additionally we observe that parameters, optimized for systems where the bulk dominates over the boundary, can be directly used for larger systems, delivering increased squeezing at larger particle numbers.

Imperfections and decoherence.—In a real experiment, optimal state preparation will be influenced by noise and imperfections. Below, we study the effect of a stochastically loaded array, and verify that the squeezing behaves smoothly under Gaussian control noise.

In general, tweezer arrays are loaded stochastically, and even with defect-removal protocols imperfections will persist. In Fig. 3 (bottom left panel) we consider a randomly half-filled 6×6 square array, and optimize the squeezer for a specific filling pattern, shown in the inset. The optimal pulse sequence is applied to various half-filling configurations. The data points show the average and standard deviation over filling realizations. Despite the inhomogeneous configuration used for optimization, considerable spin squeezing is obtained.

Noise, changing at the time scale of a single measurement, can be simulated by shot-to-shot fluctuating rotation angles and interaction times acting on the bare resources. In Fig. 3 (bottom right panel) the optimal squeezer is affected by correlated noise, independent of system size N : the application time/angle of each bare global gate suffers from the same relative error, sampled from a normal distribution with standard deviation σ_{noise} . The data points are calculated by averaging over 10 000 projective measurements each obtained from a wave function evolved under a different error realization. As expected, the impact of noise increases with the number of unitaries; thus a specific noise amplitude identifies an optimal depth n of the squeezer. Additionally we expect that a feedback-loop optimization in the presence of noise will improve these results by adjusting the optimal solution according to the noise.

To take into account the impact of spontaneous emission, we compare the interaction timescale V_0^{-1} to the effective lifetime τ_{eff} of the Rydberg-dressed excited state, through the ratio $\eta_c = V_0 \tau_{\text{eff}} = \Omega_R^2 \tau_R / (2\Delta)$, where τ_R is the lifetime of the Rydberg state. For $\tau_R \sim 50 \mu\text{s}$, $\Delta = 10\Omega_R$, and $\Omega_R = 2\pi \cdot 20 \text{ MHz}$, we expect $\eta \approx 300$. Simulations show that the total timescales $T = \sum_{i=1}^n (\tau_i + \tau'_i)$ for optimal spin squeezing are comparatively short, i.e., $TV_0 \ll \eta$, for $R_C > a$ [54], thus yielding quasicohherent evolution. In 2D they exhibit a sublinear growth with depth n . Moreover, running the quantum algorithm directly on the experimental platform automatically adjusts the optimal solution accordingly.

Outlook.—Desirable properties of the optimized SSS can be enforced by appropriately modifying the cost function [54]. Beyond that, quantum algorithms for metrology can be developed in a broader context, where the encoding, probing, decoding, and measurement steps are altogether variationally optimized. This will require efficient estimation techniques for general metrological cost functions, such as the Fisher information [71]. The quantum algorithm we presented can be readily translated for different experimental architectures, involving, e.g., molecules or optical lattices, employing their respective programmable entanglement resource to generate spin squeezing.

We thank M. Norcia, A. Young, W. Eckner, A. Elben for discussions and D. Wineland for comments on the manuscript. Work in Innsbruck is supported by the European Union’s Horizon 2020 program under Grants Agreement No. 817482 (PASQuanS) and No. 731473 (QuantERA via QTFLAG), the US Air Force Office of Scientific Research (AFOSR) via IOE Grant No. FA9550-19-1-7044 LASCEM, the Austrian Research Promotion Agency (FFG) via QFTE project AutomatiQ, by the Simons Collaboration on Ultra-Quantum Matter, which is a grant from the Simons Foundation (651440, P.Z.). Work at Boulder is supported by NIST, U.S. Army Research Office Grant No. W911NF-19-1-0223, and the U.S. AFOSR Grant No. FA9550-19-1-0275. The computational results have been achieved in part using the HPC infrastructure LEO of the University of Innsbruck and the ITensor Library.

-
- [1] H. Labuhn, D. Barredo, S. Ravets, S. de Léséleuc, T. Macrì, T. Lahaye, and A. Browaeys, *Nature (London)* **534**, 667 (2016).
- [2] H. Bernien, S. Schwartz, A. Keesling, H. Levine, A. Omran, H. Pichler, S. Choi, A. S. Zibrov, M. Endres, M. Greiner, V. Vuletić, and M. D. Lukin, *Nature (London)* **551**, 579 (2017).
- [3] L. Anderegg, L. W. Cheuk, Y. Bao, S. Burchesky, W. Ketterle, K.-K. Ni, and J. M. Doyle, *Science* **365**, 1156 (2019).
- [4] A. Cooper, J. P. Covey, I. S. Madjarov, S. G. Porsev, M. S. Safronova, and M. Endres, *Phys. Rev. X* **8**, 041055 (2018).
- [5] M. A. Norcia, A. W. Young, and A. M. Kaufman, *Phys. Rev. X* **8**, 041054 (2018).
- [6] S. Saskin, J. T. Wilson, B. Grinkemeyer, and J. D. Thompson, *Phys. Rev. Lett.* **122**, 143002 (2019).
- [7] J. P. Covey, I. S. Madjarov, A. Cooper, and M. Endres, *Phys. Rev. Lett.* **122**, 173201 (2019).
- [8] M. A. Norcia, A. W. Young, W. J. Eckner, E. Oelker, J. Ye, and A. M. Kaufman, *Science* **366**, 93 (2019).
- [9] I. S. Madjarov, A. Cooper, A. L. Shaw, J. P. Covey, V. Schkolnik, T. H. Yoon, J. R. Williams, and M. Endres, *arXiv:1908.05619*.
- [10] A. Rahmani, T. Kitagawa, E. Demler, and C. Chamon, *Phys. Rev. A* **87**, 043607 (2013).
- [11] E. Farhi, J. Goldstone, and S. Gutmann, *arXiv:1411.4028*.
- [12] A. Peruzzo, J. McClean, P. Shadbolt, M.-H. Yung, X.-Q. Zhou, P. J. Love, A. Aspuru-Guzik, and J. L. O’Brien, *Nat. Commun.* **5**, 4213 (2014).
- [13] D. Wecker, M. B. Hastings, and M. Troyer, *Phys. Rev. A* **92**, 042303 (2015).
- [14] J. R. McClean, J. Romero, R. Babbush, and A. Aspuru-Guzik, *New J. Phys.* **18**, 023023 (2016).
- [15] E. Farhi and A. W. Harrow, *arXiv:1602.07674*.
- [16] A. Kandala, A. Mezzacapo, K. Temme, M. Takita, M. Brink, J. M. Chow, and J. M. Gambetta, *Nature (London)* **549**, 242 (2017).
- [17] Y. Li and S. C. Benjamin, *Phys. Rev. X* **7**, 021050 (2017).
- [18] N. Moll, P. Barkoutsos, L. S. Bishop, J. M. Chow, A. Cross, D. J. Egger, S. Filipp, A. Fuhrer, J. M. Gambetta, M. Ganzhorn, A. Kandala, A. Mezzacapo, P. Müller, W. Riess, G. Salis, J. Smolin, I. Tavernelli, and K. Temme, *Quantum Sci. Technol.* **3**, 030503 (2018).
- [19] L. Zhou, S.-T. Wang, S. Choi, H. Pichler, and M. D. Lukin, *arXiv:1812.01041*.
- [20] C. Kokail, C. Maier, R. van Bijnen, T. Brydges, M. K. Joshi, P. Jurcevic, C. A. Muschik, P. Silvi, R. Blatt, C. F. Roos, and P. Zoller, *Nature (London)* **569**, 355 (2019).
- [21] N. Klco, E. Dumitrescu, A. McCaskey, T. Morris, R. Pooser, M. Sanz, E. Solano, P. Lougovski, and M. Savage, *Phys. Rev. A* **98**, 032331 (2018).
- [22] H. Pichler, S.-T. Wang, L. Zhou, S. Choi, and M. D. Lukin, *arXiv:1808.10816*.
- [23] V. Giovannetti, S. Lloyd, and L. Maccone, *Science* **306**, 1330 (2004).
- [24] L. Pezzè, A. Smerzi, M. K. Oberthaler, R. Schmied, and P. Treutlein, *Rev. Mod. Phys.* **90**, 035005 (2018).
- [25] Performing occasional reoptimization steps, via a local search algorithm starting from the previous optimal solution, can account for low frequency noise, fluctuating at timescales longer than the optimization runtime (slow drifts in the experimental quantities).
- [26] P. J. J. O’Malley *et al.*, *Phys. Rev. X* **6**, 031007 (2016).
- [27] O. de Mello, D. Schäffner, J. Werkmann, T. Preuschoff, L. Kohfahl, M. Schlosser, and G. Birkel, *Phys. Rev. Lett.* **122**, 203601 (2019).
- [28] D. J. Wineland, J. J. Bollinger, W. M. Itano, F. L. Moore, and D. J. Heinzen, *Phys. Rev. A* **46**, R6797 (1992).
- [29] M. Kitagawa and M. Ueda, *Phys. Rev. A* **47**, 5138 (1993).
- [30] C. A. Sackett, D. Kielpinski, B. E. King, C. Langer, V. Meyer, C. J. Myatt, M. Rowe, Q. A. Turchette, W. M. Itano, D. J. Wineland, and C. Monroe, *Nature (London)* **404**, 256 (2000).
- [31] D. Leibfried, E. Knill, S. Seidelin, J. Britton, R. B. Blakestad, J. Chiaverini, D. B. Hume, W. M. Itano, J. D. Jost, C. Langer, R. Ozeri, R. Reichle, and D. J. Wineland, *Nature (London)* **438**, 639 (2005).
- [32] T. Monz, P. Schindler, J. T. Barreiro, M. Chwalla, D. Nigg, W. A. Coish, M. Harlander, W. Hänsel, M. Hennrich, and R. Blatt, *Phys. Rev. Lett.* **106**, 130506 (2011).
- [33] J. G. Bohnet, B. C. Sawyer, J. W. Britton, M. L. Wall, A. M. Rey, M. Foss-Feig, and J. J. Bollinger, *Science* **352**, 1297 (2016).
- [34] J. Estève, C. Gross, A. Weller, S. Giovanazzi, and M. K. Oberthaler, *Nature (London)* **455**, 1216 (2008).

- [35] M. F. Riedel, P. Böhi, Y. Li, T. W. Hänsch, A. Sinatra, and P. Treutlein, *Nature (London)* **464**, 1170 (2010).
- [36] B. Lücke, M. Scherer, J. Kruse, L. Pezzé, F. Deuretzbacher, P. Hyllus, O. Topic, J. Peise, W. Ertmer, J. Arlt, L. Santos, A. Smerzi, and C. Klempt, *Science* **334**, 773 (2011).
- [37] C. D. Hamley, C. S. Gerving, T. M. Hoang, E. M. Bookjans, and M. S. Chapman, *Nat. Phys.* **8**, 305 (2012).
- [38] T. Berrada, S. van Frank, R. Bücker, T. Schumm, J.-F. Schaff, and J. Schmiedmayer, *Nat. Commun.* **4**, 2077 (2013).
- [39] Y.-Q. Zou, L.-N. Wu, Q. Liu, X.-Y. Luo, S.-F. Guo, J.-H. Cao, M. K. Tey, and L. You, *Proc. Natl. Acad. Sci. U.S.A.* **115**, 6381 (2018).
- [40] J. Appel, P. J. Windpassinger, D. Oblak, U. B. Hoff, N. Kjærgaard, and E. S. Polzik, *Proc. Natl. Acad. Sci. U.S.A.* **106**, 10960 (2009).
- [41] I. D. Leroux, M. H. Schleier-Smith, and V. Vuletić, *Phys. Rev. Lett.* **104**, 073602 (2010).
- [42] Z. Chen, J. G. Bohnet, J. M. Weiner, K. C. Cox, and J. K. Thompson, *Phys. Rev. A* **89**, 043837 (2014).
- [43] R. J. Sewell, M. Napolitano, N. Behbood, G. Colangelo, F. Martin Ciurana, and M. W. Mitchell, *Phys. Rev. X* **4**, 021045 (2014).
- [44] G. Barontini, L. Hohmann, F. Haas, J. Estève, and J. Reichel, *Science* **349**, 1317 (2015).
- [45] O. Hosten, N. J. Engelsen, R. Krishnakumar, and M. A. Kasevich, *Nature (London)* **529**, 505 (2016).
- [46] L. I. R. Gil, R. Mukherjee, E. M. Bridge, M. P. A. Jones, and T. Pohl, *Phys. Rev. Lett.* **112**, 103601 (2014).
- [47] Y. C. Liu, Z. F. Xu, G. R. Jin, and L. You, *Phys. Rev. Lett.* **107**, 013601 (2011).
- [48] C. Shen and L.-M. Duan, *Phys. Rev. A* **87**, 051801(R) (2013).
- [49] J.-Y. Zhang, X.-F. Zhou, G.-C. Guo, and Z.-W. Zhou, *Phys. Rev. A* **90**, 013604 (2014).
- [50] T. Pichler, T. Caneva, S. Montangero, M. D. Lukin, and T. Calarco, *Phys. Rev. A* **93**, 013851 (2016).
- [51] I. Bouchoule and K. Mølmer, *Phys. Rev. A* **65**, 041803(R) (2002).
- [52] C. Brif and A. Mann, *Phys. Rev. A* **54**, 4505 (1996).
- [53] A. S. Sørensen and K. Mølmer, *Phys. Rev. Lett.* **86**, 4431 (2001).
- [54] See Supplemental Material at <http://link.aps.org/supplemental/10.1103/PhysRevLett.123.260505> for additional details.
- [55] A. D. Ludlow, M. M. Boyd, J. Ye, E. Peik, and P. O. Schmidt, *Rev. Mod. Phys.* **87**, 637 (2015).
- [56] S. L. Campbell, R. B. Hutson, G. E. Marti, A. Goban, N. Darkwah Oppong, R. L. McNally, L. Sonderhouse, J. M. Robinson, W. Zhang, B. J. Bloom, and J. Ye, *Science* **358**, 90 (2017).
- [57] N. Henkel, R. Nath, and T. Pohl, *Phys. Rev. Lett.* **104**, 195302 (2010).
- [58] G. Pupillo, A. Micheli, M. Boninsegni, I. Lesanovsky, and P. Zoller, *Phys. Rev. Lett.* **104**, 223002 (2010).
- [59] J. Honer, H. Weimer, T. Pfau, and H. P. Büchler, *Phys. Rev. Lett.* **105**, 160404 (2010).
- [60] J. E. Johnson and S. L. Rolston, *Phys. Rev. A* **82**, 033412 (2010).
- [61] Y.-Y. Jau, A. M. Hankin, T. Keating, I. H. Deutsch, and G. W. Biedermann, *Nat. Phys.* **12**, 71 (2016).
- [62] J. Zeiher, R. van Bijnen, P. Schauß, S. Hild, J.-y. Choi, T. Pohl, I. Bloch, and C. Gross, *Nat. Phys.* **12**, 1095 (2016).
- [63] J. Zeiher, J. Y. Choi, A. Rubio-Abadal, T. Pohl, R. van Bijnen, I. Bloch, and C. Gross, *Phys. Rev. X* **7**, 041063 (2017).
- [64] A. D. Bounds, N. C. Jackson, R. K. Hanley, R. Faoro, E. M. Bridge, P. Huillery, and M. P. A. Jones, *Phys. Rev. Lett.* **120**, 183401 (2018).
- [65] A. Arias, G. Lochead, T. M. Wintermantel, S. Helmrich, and S. Whitlock, *Phys. Rev. Lett.* **122**, 053601 (2019).
- [66] H. Strobel, W. Muessel, D. Linnemann, T. Zibold, D. B. Hume, L. Pezzè, A. Smerzi, and M. K. Oberthaler, *Science* **345**, 424 (2014).
- [67] D. R. Jones, C. D. Perttunen, and B. E. Stuckman, *J. Optim. Theory Appl.* **79**, 157 (1993).
- [68] D. Finkel and C. Kelley, *Optimization Online* **14**, 1 (2004), <https://projects.ncsu.edu/crsc/reports/ftp/pdf/crsc-tr04-28.pdf>.
- [69] P. E. Nicholas, in *Proceedings of the 14th INFORMS Computing Society Conference*, Vol. 14 (2014), p. 47, <https://www.informs.org/Publications/ICS-Proceedings/2015-Conference-Volume/ICS-2015-Table-of-Contents>.
- [70] H. Liu, S. Xu, X. Wang, J. Wu, and Y. Song, *Eng. Optim.* **47**, 1441 (2015).
- [71] S. L. Braunstein and C. M. Caves, *Phys. Rev. Lett.* **72**, 3439 (1994).
- [72] P. Hyllus, W. Laskowski, R. Krischek, C. Schwemmer, W. Wiecek, H. Weinfurter, L. Pezzé, and A. Smerzi, *Phys. Rev. A* **85**, 022321 (2012).
- [73] G. Tóth, *Phys. Rev. A* **85**, 022322 (2012).
- [74] M. Foss-Feig, Z.-X. Gong, A. V. Gorshkov, and C. W. Clark, [arXiv:1612.07805](https://arxiv.org/abs/1612.07805).
- [75] M. P. Zaletel, R. S. K. Mong, C. Karrasch, J. E. Moore, and F. Pollmann, *Phys. Rev. B* **91**, 165112 (2015).